Chemical Science

ROYAL SOCIETY OF CHEMISTRY

EDGE ARTICLE

View Article Online
View Journal | View Issue

Cite this: *Chem. Sci.*, 2022, **13**, 10308

All publication charges for this article have been paid for by the Royal Society of Chemistry

Received 4th July 2022
Accepted 12th August 2022

DOI: 10.1039/d2sc03729g

rsc.li/chemical-science

Deformation-induced phosphorescence shift in a 2D elastically flexible organic single crystal: role of chalcogen-centered weak interactions†

Subhrajyoti Bhandary, [a] Rik Van Deun, [b] Anna M. Kaczmarek [c] and Kristof Van Hecke *[a]

Mechanically responsive organic luminescent crystals are one of the promising choices of materials for flexible photonic devices. However, the change in phosphorescence emission as a function of the flexibility of a crystal has never been reported. Our current findings demonstrate two-dimensional (2D) and one-dimensional (1D) macroscopic elastic deformability, under mechanical stress, in elastically flexible single crystals of dibenzothiophene, and its brominated derivative, respectively. Unlike the presence of dual fluorescence (FL) and room temperature phosphorescence (RTP) in dibenzothiophene single crystals, the derivative was found to show only RTP. Interestingly, upon elastic deformation, single crystals of the dual emissive dibenzothiophene show a noticeable blue shift (~20 nm) of RTP emission when compared to their pristine crystals (straight and naturally bent). However, their FL peaks remain nearly unchanged irrespective of the crystal deformation. A hierarchy of structure-elastic functionality to RTP modulation has been quantitatively mapped by rationalizing the role of chalcogen-involved weak interactions.

Introduction

Molecular single crystals that can be mechanically reconfigured without losing the long-range intrinsic order are part of the core research in materials science and crystal engineering.[1] In recent years, there have been plenty of examples reported which show that molecular crystals can be elastically (reversibly) and plastically (permanently) deformed, exceptionally at a macroscopic level when subjected to mechanical force.[1–3] Such impressive mechanical adaptability in organic crystals opens a new window of opportunity for their potential use in smart flexible displays, optoelectronic devices, optical sensors, and so on.[4] In this regard, organic single crystals, showing luminescence as well as mechanically compliant behavior, are of particular interest. For instance, such soft organic single crystals, which can alter their emission properties by adopting different shapes under external mechanical force, are of relevance to sensing and flexible display applications.[5] Indeed, these responsive soft crystals are different from conventional mechanochromic (fluorescence/phosphoresce) materials, which mostly respond to anisotropic grinding and isotropic pressure.[6] In the current context, mechanical bending, causing FL modifications in elastically,[5a,b] as well as plastically[5c] flexible single crystals, has been reported. The Takamizawa group reported reversible fluorochromism in a superelastic crystal.[5d] Zhang and co-workers have recently found a rare incident of FL blue shifting, by applying tensile forces, in an elasto-plastic crystal.[5e] Conversely, the adjustment of RTP emission in mechanically adaptable (plastic/elastic) molecular single crystals has not yet been explored. In fact, organic RTP crystals, integrated with reversible bending features, could be more promising candidates for flexible waveguide and display devices.[7] However, dual-functional RTP and elastic softness, within a single crystal, are extremely rare. To the best of our knowledge, to date, only few elastic RTP organic crystals have been identified, namely dibromobenzil,[7b] three halogenated triazine–carbazole derivatives,[8a] and a phenothiazine analogue.[8b] Also, all of them are 1D elastically flexible, while a 2D elastically responsive RTP crystal has not yet been reported. This is because the design of RTP metal-free single-component ordered molecular materials is still in its infancy.[7] Concurrently, tremendous efforts have already been directed in designing elastically flexible molecular crystals in the last decade.[5a,9] Generally, the presence of uniformly distributed weak interactions, polarizable halogen bonds (σ-hole type), π-hole, halogen-centered contacts, π···π stacking, and weak hydrogen bonds in organic crystals can act

[a]*XStruct, Department of Chemistry, Ghent University, Krijgslaan 281-S3, 9000 Ghent, Belgium. E-mail: kristof.vanhecke@ugent.be*

[b]*L^3 – Luminescent Lanthanide Lab, Department of Chemistry, Ghent University, Krijgslaan 281-S3, 9000 Ghent, Belgium*

[c]*NanoSensing Group, Department of Chemistry, Ghent University, Krijgslaan 281-S3, 9000 Ghent, Belgium*

† Electronic supplementary information (ESI) available: Materials, crystallographic and photoluminescence studies. CCDC 2120853, 2120854, 2166317 and 2166318. For ESI and crystallographic data in CIF or other electronic format see **https://doi.org/10.1039/d2sc03729g**

as a structural buffer for exhibiting elastic properties.[1c,9b,c,10] It has also been suggested that π-extended fluorescent molecules, having planar locked geometry and strong displaced stacking interactions, promote elasticity in crystals.[5a,10] Certainly, modern microfocus synchrotron diffraction mapping further enriches our understanding on the mechanism of elastic deformation in molecular crystals.[2a,3a,11] However, the proposed supramolecular structural conditions for the origin of elasticity in crystalline materials are yet still largely system specific. Hence, the elasticity integrated with RTP phenomenon in molecular single crystals deserves more attention with a diverse range of examples to elucidate the role of various types of noncovalent interactions that can influence such appealing properties.

Here, we present 2D elastic performance in single crystals of dibenzothiophene (DBS) and 1D elastic flexibility of 2-bromodibenzothiophene (DBS–Br) crystals (Fig. 1) under applied mechanical stress. DBS is one of the earliest known crystallization-induced dual FL and RTP metal-free materials.[12,13a] The inclusion of thiophene moieties and chalcogen atoms have emerged as a desirable class of structural core for the design of new persistent RTP metal-free crystalline materials.[13] Moreover, the findings on dual-functional elasticity and fluorescence properties in single crystals of thiophene core-containing extended π-conjugated molecules include a new dimension to the advancement of luminescent flexible crystals.[5a,10] In the current case, flexible single crystals of DBS–Br were also found to show RTP properties. Importantly, the elastically bent single crystals of DBS show an evident switching of their RTP emission peak (blue shifted) when compared to their pristine undeformed or naturally bent crystals.

Results and discussion

The crystallization of both compounds (DBS and DBS–Br) in various organic solvents results in acicular/long-plate shaped, straight, as well as naturally deformed, crystals (Fig. 1c–e). It must be noted that the crystal structure of the DBS–Br has not been reported yet. The single-crystal X-ray diffraction (SCXRD) data of suitable straight crystals has been collected for both DBS and DBS–Br (Table S1 and Fig. S1 and S2†). The phase purity of the crystal batches was validated using powder X-ray diffraction (Fig. S3†). The supramolecular packing of the planar DBS and DBS–Br molecules is displayed in Fig. 2, and a list of possible interactions along with geometrical criteria is provided in Table S2.† The structural features of DBS ($P2_1/n$, $Z = 4$) demonstrate that the crystal packing (Fig. 2a) is interlocked from major faces (101)/(−10−1). On (010)/(0−10), two oppositely orientated DBS molecules are connected to each other *via* different less-directional C–H···π interactions (Fig. 2b). Moreover, the sulfur involved C–H···S (2.99 Å, 165°) and relatively directional S(σ-hole)···π motif (3.58 Å, 149°) associated with C–H···π interactions (shaded in orange and blue, respectively), stabilize cofacial molecules forming a molecular ribbon along [001]. Such DBS molecules are further stacked in displaced fashion *via* S···π (3.63–3.71 Å) interactions on the (001)/(00−1) faces and extended along [010], creating molecular layers (shaded in blue, Fig. 2c). On the contrary, DBS–Br molecules form zig-zag layers along [100], as viewed from their major faces (001)/(00−1) of the crystal (Fig. 2d). Like DBS, the arrangement of molecules in the DBS–Br crystal ($P2_12_12_1$, $Z = 4$) is also primarily guided by sulfur involved directional C–H···S (2.92–3.08 Å, 163–166°, shaded in orange, Fig. 2e) and C–H···π interactions associated with C–H···Br hydrogen bonds. The lateral (011) face of the crystal displays stacking of DBS–Br molecules along [100] by S···π (3.57 Å) and π···π (3.57 Å) interactions, forming layers parallel with the *a*-axis (shaded blue, Fig. 2f).

The straight shaped single crystals (∼2–3 mm long, acicular) of both DBS and DBS–Br have been observed to be mechanically flexible (Fig. 3). At ambient temperature (18–25 °C), DBS single crystals could be macroscopically bent into a semi-circular arc, down the major face (*i.e.* the (101)/(−10−1) plane) using a three-point support of a pair of tweezers and needle (Fig. 3a and Movies S1 and S2†). The original straight shape could also be successfully restored upon relaxation of force, which is indicative of elastic deformation (see ESI† for bending experiments). The process of bending and subsequent shape restoration can be performed in a loop without breaking the single crystals. Remarkably, the DBS crystals also display elastic flexibility from the lateral faces (001)/(00−1), however, to a lesser extent in comparison to the major (101)/(−10−1) faces (Fig. 3c and Movies S3 and S4†). Hence, DBS crystals can be categorized as 2D elastically flexible organic crystals. Similarly, DBS–Br single crystals could only be deformed into an arc down the major faces (001)/(00-1), which is followed by shape recovery upon removal of stress (Fig. 3b and Movie S5†). The DBS–Br crystals are bendable from 1D and are brittle from lateral (011)/(0−1−1) faces (Movie S6†). However, beyond a certain onset of deformation, the crystals are fragmented for both compounds. We did not observe any stress-induced permanent (plastic) deformation for single crystals of both compounds.

The naturally bent (from their major faces) as grown crystals of both molecules also display behavior when subjected to similar mechanical stress. Furthermore, the crystal structures of such naturally deformed DBS and DBS–Br crystals have been

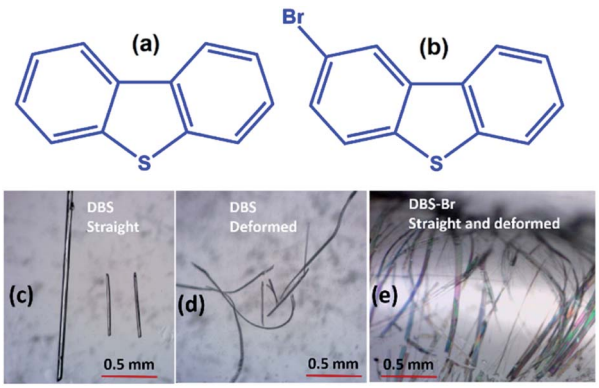

Fig. 1 Chemical structures of DBS (a) and DBS–Br (b). Different morphologies (straight and deformed) of as grown crystals (c–e). Both DBS and DBS–Br crystallize as a mixture of straight and deformed crystals.

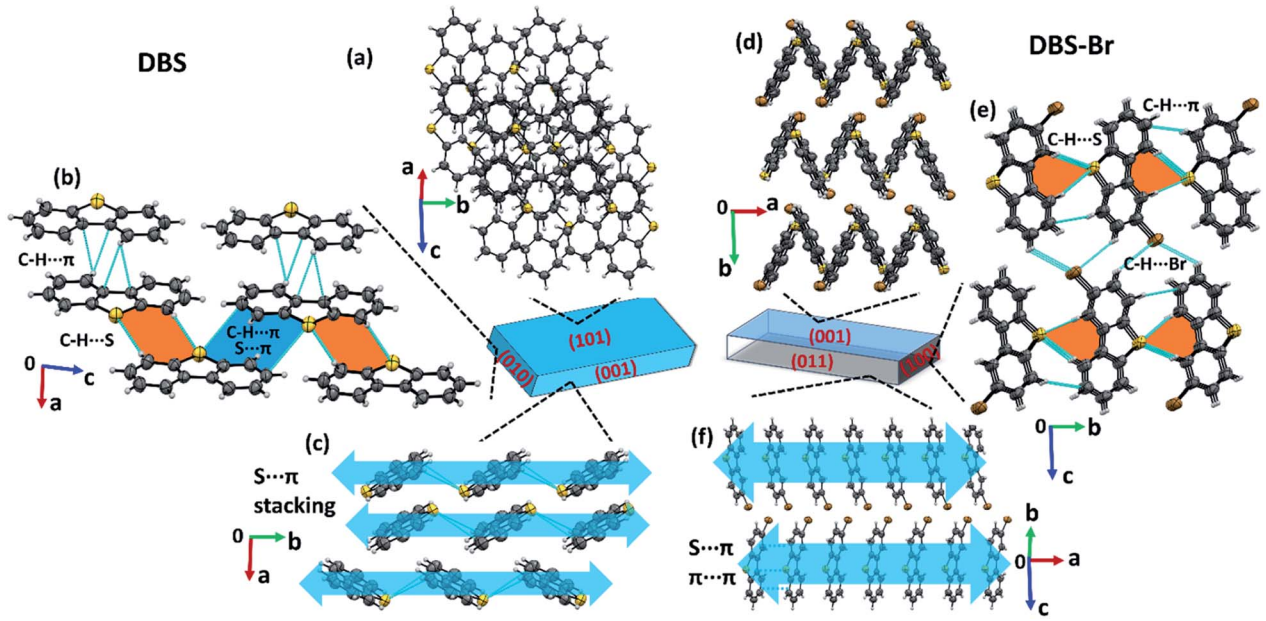

Fig. 2 Packing arrangement of molecules in different faces of DBS (a–c) and DBS–Br (d–f) single crystals. Orange and blue shades depict sulfur centered C–H···S and S···π stacking interactions, respectively.

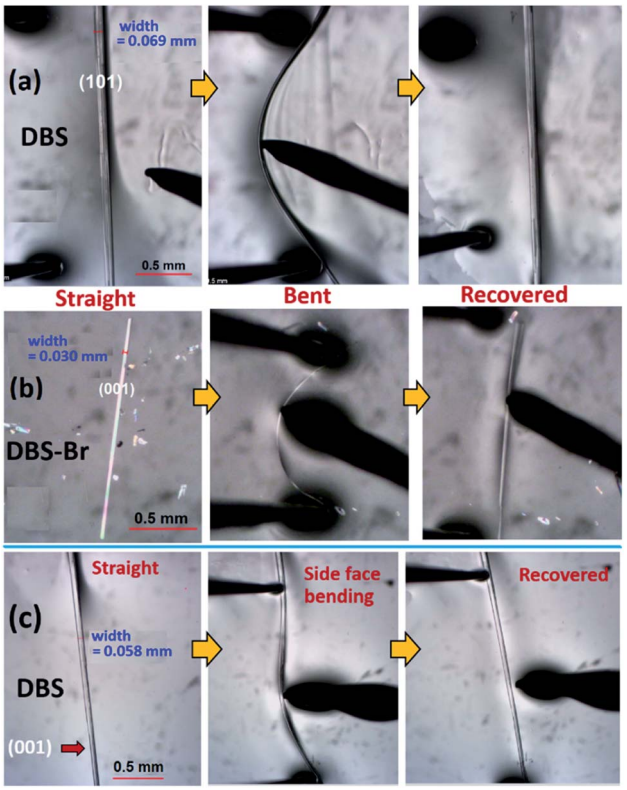

Fig. 3 Elastic bending and subsequent recovery process for (a) DBS and (b) DBS–Br single crystals on their major faces under an Olympus SZ61-TR optical microscope by three-point bending. (c) Elastic bending of a DBS crystal on side faces (001)/(00−1).

determined by SCXRD analysis, which shows no change in structural parameters when compared to their respective straight shape crystals (Table S1†). It has also been realized that the single crystallinity of naturally grown bent crystals (at the bent region) is slightly compromised in comparison with their straight counterparts, *i.e.* the deformed crystals clearly result in relatively less precise X-ray diffraction data without having any structural change in comparison to their straight crystals (Table S1†). Moreover, the intrinsic integrity of DBS single crystals upon elastic bending has also been confirmed by mounting an elastically deformed (from major face) single crystal on a home source single-crystal X-ray diffractometer. The observed diffraction spots at low angles (weak in intensity and broad) at the bent region of the crystal clearly indicate the preservation of single crystallinity upon elastic bending (Fig. S4†).

The elastic strain of single crystals of both compounds at their maximum deformation limit was calculated by the Euler–Bernoulli equation[14] (see ESI† for details, Fig. S5–S7†). The elastic strain on the major faces of DBS (101)/(−10−1) and DBS–Br (001)/(00−1) were measured to be around 3.3% and 2.5%, respectively. This suggests that DBS crystals from major faces can accommodate more stress in comparison to DBS–Br. However, the elastic bending ability from the lateral faces (001)/(00−1) of DBS crystals are calculated to be around 0.8% only.

Photoluminescence (PL) characterization of one straight single crystal (acicular) of each compound suggests that they both show weak RTP in the solid-state (see ESI† for details). The RTP emission peaks, for DBS and DBS–Br single crystals, were detected approximately at 563 nm (lifetime of 11.6 μs) and 441 nm (lifetime of 8.7 μs), respectively (Fig. S8–S11 and Table S3†). Moreover, the pristine straight single crystal (~4 mm long) of DBS showed dual FL (peak at *ca.* 356 nm) and RTP (peak at *ca.* 563 nm) emission phenomena (Fig. 4), which corroborates with previous reports.[12,13a] In order to investigate the effect of stress on FL and RTP emissions, for differently manipulated DBS single crystals, we recorded PL spectra for a pristine straight, an

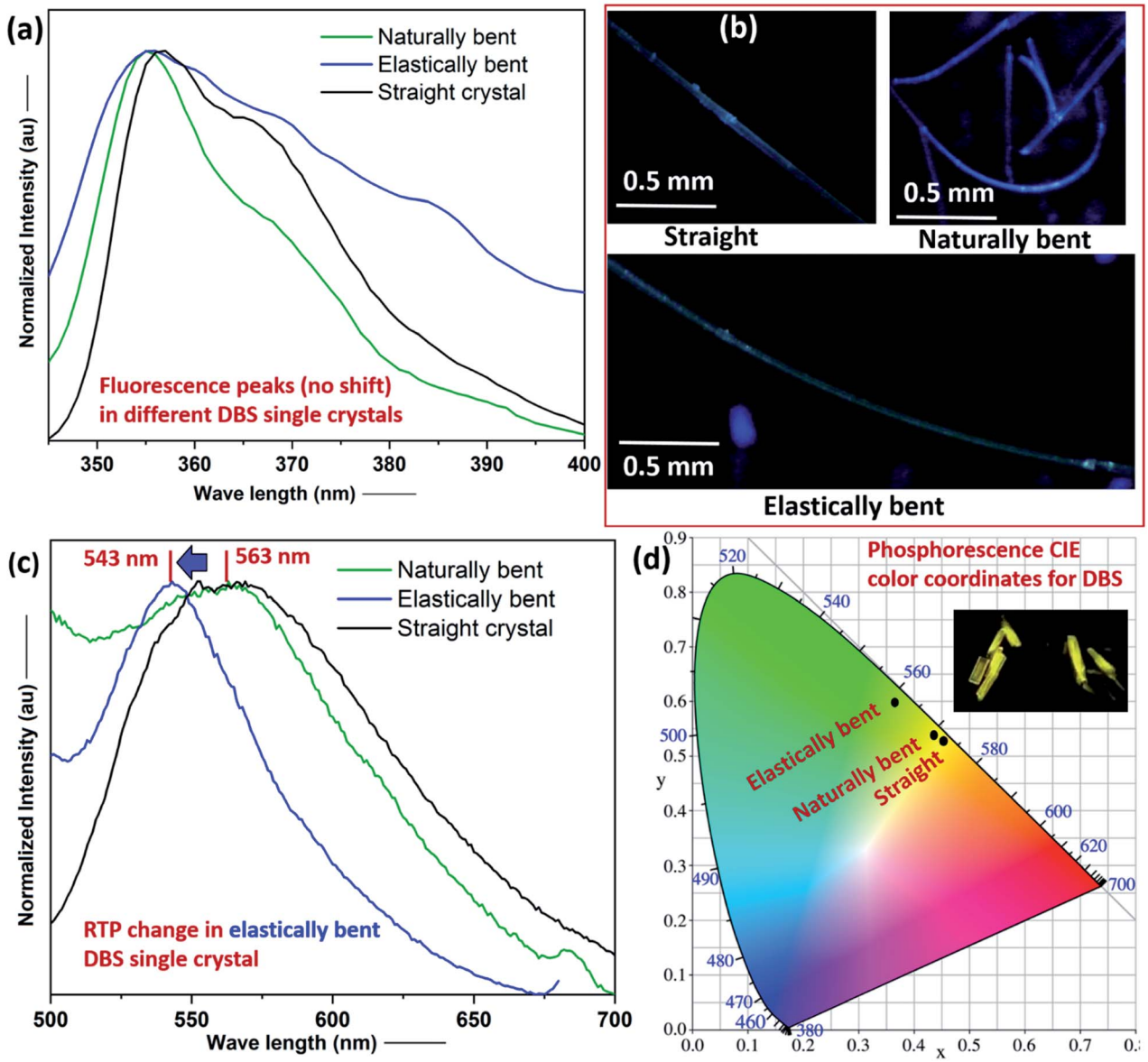

Fig. 4 (a) Fluorescence spectra (peak maximum at 356 nm) of a straight (black), a naturally bent (green) and an elastically bent (blue) DBS single crystal. (b) Photographic images of differently shaped blue-emissive DBS single crystals under 365 nm UV excitation. (c) RTP emission spectra, showing a hypsochromic shift of the RTP emission peak (563 nm to 543 nm) for an elastically bent single crystal (blue spectrum) of DBS. (d) Corresponding CIE color coordinates for the RTP emission of DBS crystals and yellow afterglow of straight crystals (inset). Single crystals were excited at λ_{ex} = 300 nm, using a xenon lamp for all PL measurements.

elastically bent and a naturally bent single crystal (Fig. S12†).[15] All three DBS single crystals display a FL peak approximately at 356 nm, which means there is no prominent effect of mechanical bending on the FL spectra of DBS crystals (Fig. 4a), although a broadening of the PL spectrum of the elastically bent DBS crystal is noticed, which could possibly be attributed to an increase of local defects within the DBS single crystal lattice (inhomogeneous long-range order), due to the employed elastic deformation. The straight, naturally deformed, and elastically bent single crystals are blue emissive under a 365 nm UV lamp (Fig. 4b). Interestingly, a closer look of their RTP spectra clearly indicates a blue shifting (maximum shift from 563 nm to 543 nm) of the emission peak for the elastically deformed crystal in comparison to the pristine straight and naturally bent crystals (Fig. 4c). The shifted RTP peak was observed to return to the initial position after removing stress from the elastically deformed crystal, however, performing switching cycle (fatigue) experiments were not possible for the same crystal, as the DBS single crystals were not found to be sustainable (breaking) after multiple elastic bending experiments, depending on their size and morphology. Furthermore, the plot of their CIE color coordinates also reveals the modification of the RTP emission from the yellow (inset) to green region on the account of elastic deformation in DBS crystals (Fig. 4d).

The origin of the observed impressive 2D/1D elastic flexibilities of both compounds and observed RTP change in the deformed DBS single crystals can be rationalized from the quantification of their supramolecular features and interaction topology. Therefore, we first computed molecular electrostatic potential (ESP) maps and energy frameworks (based on pairwise interaction energy) for both π-surfaced molecules using CrystalExplorer17.5,[16,17] at the CE-B3LYP/DGDZVP level of theory (Fig. 5). The ESP plot of DBS (Fig. 5a) indicates two highly electron rich phenyl rings (red, ESP ranges from −49.0 to −52.5 kJ mol^{-1}) and a relatively less electron dense thiophene core (ESP of −26.0 kJ mol^{-1}). In the case of DBS–Br (Fig. 5b), the addition of a heavy halogen atom significantly modifies the ESP distributions in the molecule. Two phenyl rings become less rich and anisotropic (−21 kJ mol^{-1} and −31.5 kJ mol^{-1}) compared to the former. Moreover, the formation of an electron deficient π-hole[18a] on the thiophene surface of DBS–Br is notable (see blue positive surface, ESP of 13.4 kJ mol^{-1}). It is now clear that the DBS–Br molecules are more prone to form stacking interactions between aromatic rings for better electrostatic complementarity between phenyl and thiophene units compared to DBS. For this reason, weak slip stacking of molecules has been favored in DBS crystals (through S⋯π contacts to minimize repulsion among π-rings) having an interaction energy (IE) of −16.1 kJ mol^{-1} (side face in Fig. 2c). In the case of DBS–Br, a stronger stacking (IE −36.7 kJ mol^{-1}) is associated with S⋯π (hole) and π⋯π interactions (see side face packing in Fig. 2f). Another intriguing fact about the ESP plots here is the presence of two small electron deficient σ-holes[18] (black arrows, blue regions) on light chalcogen atoms (S) for both DBS and DBS–Br crystals (ESP ranges from 36.6 to 39.0 kJ mol^{-1}). A weak σ-hole on the Br atom is also observed (ESP of 33.8 kJ mol^{-1}). However, such σ-holes on chalcogen mostly remain unutilized by molecules in both crystals except for the formation of C–H⋯π supported relatively directional S(σ-hole)⋯π (IE −13.4 kJ mol^{-1}) interactions in DBS (shaded ribbons in Fig. 2b). Furthermore, the computed energy framework[17] of DBS (Fig. 5c) depicts a nearly hexagonal interaction topology (represented by cylindrical tubes) down the ac-crystallographic plane, constructed mostly through C–H⋯π (IE −26.0 kJ mol^{-1}), π⋯π stacking (−20.6 kJ mol^{-1}), and C–H⋯π supported S(σ-hole)⋯π interactions (−13.4 kJ mol^{-1}). Furthermore, the S⋯π guided displaced stacking along the needle axis of the crystal [010], having an IE of −16.1 kJ mol^{-1}, makes the energetic topology nearly isotropic in terms of its comparable strength. Within this unique hexagonal isotropic topology of DBS, the cooperative interplay of C–H⋯π (dimeric motifs along the major face (101)) and different S-involved (S⋯π and C–H⋯S) interactions along [001] of the crystal (see shaded ribbons in Fig. 2b) could be the origin for exhibiting 2D elastic macroscopic flexibilities from both faces of the crystal. Unlike DBS, an anisotropic energetic topology has been evident in DBS–Br crystals, which is primarily stabilized by relatively strong (S⋯π(hole) stacking, −36.7 kJ mol^{-1}, thicker tubes) *vs.* weak (C–H⋯S, −15.4/−14.7 kJ mol^{-1}, thin tubes) interactions in nearly orthogonal fashion (Fig. 5d). Despite this anisotropic interaction topology, the manifestation of structure-guiding S⋯π-hole associated stacking and C–H⋯S dimers is capable to promote elastic bending in DBS–Br single crystals on major faces (001/00−1) only. We hypothesize that such chalcogen-involved (σ/π-holes) interactions in both DBS and DBS–Br crystals can act as a restorative force for the reversible bending through accommodating the applied stress within their stacking columns by the expansion-contraction fashion (Fig. 6 and S13†).

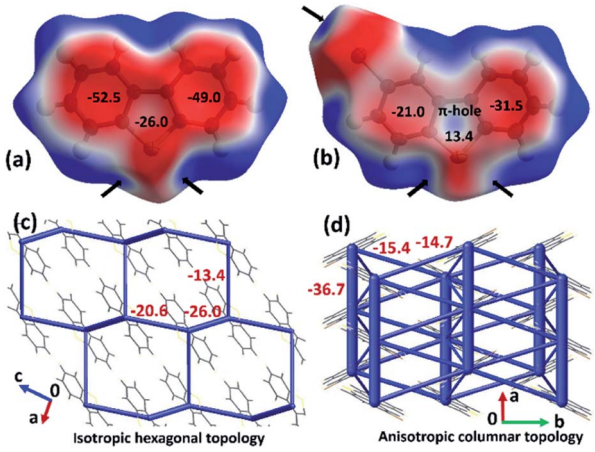

Fig. 5 Molecular electrostatic potential (ESP) plots for (a) DBS and (b) DBS–Br crystals mapped with a color scale of <−40.0 kJ mol^{-1} (all red) to >40.0 kJ mol^{-1} (all blue). Computed energy frameworks show hexagonal topology for DBS (c), and columnar topology for DBS–Br (d) crystals. ESP of the rings and IE in frameworks (in kJ mol^{-1}) are emphasized. Black arrows in ESP plots indicate σ-holes. Thicker cylindrical tubes represent relatively stronger interactions in the energy frameworks.

It is worth stating that the chalcogen-involved intermolecular interactions (various σ/π-hole types S⋯π, and C–H⋯S) and associated molecular stacking also plays a central role in the generation of RTP properties in both DBS and DBS–Br crystals. This could be rationalized in terms of efficient intersystem crossing (*via* n–π* type transition) guided by hetero-chalcogen atoms[13c] and various S-associated intermolecular interactions that restrict the molecular motion in both crystals. Moreover, the electrostatic nature of different σ/π hole driven S⋯π interactions may contribute to a similar effect (intermolecular electron coupling and restricted molecular motion) to RTP as halogen bonding.[18b,19a] It is also recognized that the face-to-face aromatic π⋯π stacking and introduction of hetero S-atoms may endorse the mechanophosphorescence process in crystals.[6b,c,19] In DBS crystals, the displaced stacking columns are primarily stabilized by hetero-atom mediated S⋯π interactions, avoiding pure (face-to-face) π⋯π stacking along the needle axis of the crystal (blue arrows in Fig. 2c). During elastic bending of a crystal having a planar molecular core[11] like DBS, there must be a local variation of packing patterns within the stacking columns across the bend of the acicular crystal (Fig. 6 and S13†). Such reorganization of stacking patterns upon bending could be feasible *via* redistribution of the weak S⋯π (energetically less demanding, IE −16.1 kJ mol^{-1}) interactions *via* reversible rotation of DBS molecules across the bend (black arrows in Fig. 6). In effect, the stacking column of DBS

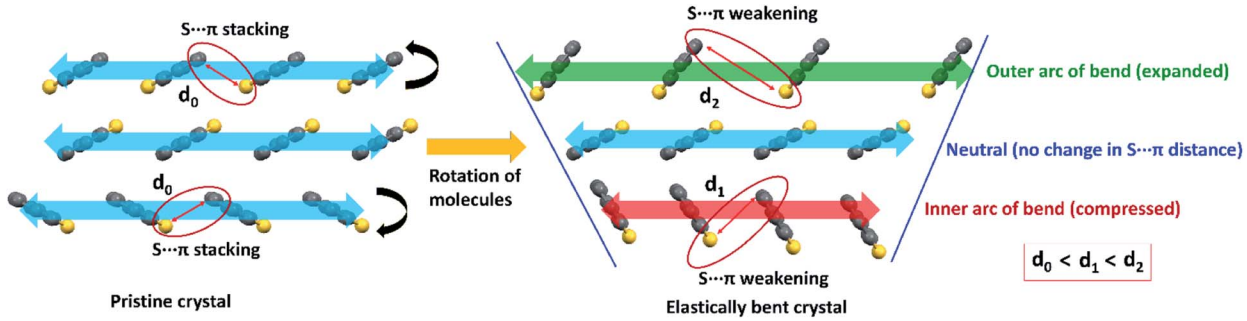

Fig. 6 A possible molecular level change of stacking columns of DBS molecules upon elastic bending of a pristine DBS crystal on its major face, showing the weakening (stretching) of S···π interactions (face-to-edge S···C distance between adjacent molecules) because of reversible rotation of molecules (black arrows) to result in a contracted inner (red in color) to expanded outer (green) arc of the bent region. The stretching of S···π distance in the outer side is greater than the inner side of the bend ($d_0 < d_1 < d_2$) due to a larger molecule-to-molecule separation in the former region. Note that stacking columns extend along the needle axis (*b*-axis) of crystals as shown in Fig. 2c.

molecules in the outer arc of the bend would be expanded and subsequent contraction of molecule-to-molecule stacking distance is expected in the inner part to accommodate the stress (Fig. 6). Despite the expansion and contraction of intermolecular stacking columns from outer to inner columns upon bending, the rotation of DBS molecules across the bend (black arrows) causes a larger face-to-edge S···C separation of molecules ($d_0 < d_1 < d_2$, Fig. 6) which subsequently weakens S···π interactions in crystal. Hence, on bending, the stretching of S···π distances in both outer and inner arc of stacked DBS columns, could be the primary reason for the observed hypsochromic shift of RTP emission peak. Furthermore, it has previously been realized that the adjustment of pure π···π stacking distances upon bending causes macroscopic changes in FL emission for flexible crystals.[5c,e] In the current case, S···π associated columns (displaced stacking) have minor contributions from pure π···π interactions of DBS rings due to electrostatic reasons (reduce repulsion) and hence, it is expected to influence less likely the FL peak of DBS upon mechanical bending.

To get further insight into the importance of such chalcogen-cantered interactions in mechanical-emission properties, we analyzed the crystal structures of well-known elastically bendable luminescent π-conjugated crystals having thiophene moieties.[5a,10] Such investigation also suggested that in addition to the displaced stacking, the S-centered weak interactions (*e.g.*, S···F, S···π, S···S, and C–H···S) have also been noticed to play a crucial role in their interaction topologies (Fig. S14†).

Conclusions

In conclusion, we have revealed 2D elastic bendability under applied stress in well-known dual emissive (FL and RTP) dibenzothiophene single crystals, whereas 1D reversible flexibility has been recognized for their RTP Br-derivatives. We also found a unique hypsochromic shift (~20 nm) of the RTP emission peak for DBS single crystals as a consequence of elastic bending when compared to their pristine and naturally deformed crystals. In contrast, no prominent changes were detected in the FL spectra for such manipulated crystal shapes. Remarkably, this is the first finding of an elastically flexible crystal that shows a clear mechanophosphorescence effect upon bending. The structural features, together with their energetic topologies, established that different chalcogen-centered weak interactions (*e.g.*, various σ/π-hole type S···π, and C–H···S) play a critical role in originating both impressive elastic deformability and RTP properties in two compounds. Furthermore, the evident blue shift of the RTP emission peak in case of an elastically deformed DBS crystal is attributed to the weakening of hetero atom-involving (S···π) interactions of molecules that occurs during bending. We postulate these weak S-centered interactions, including chalcogen bonds,[18b] will be exploited in the future for the rational design of RTP based mechanically soft crystalline materials towards their photonic applications.

Data availability

All experimental, crystallographic, and computational data are available in the ESI.†

Author contributions

K. V. H. designed and supervised the project. S. B. and A. M. K. performed the experiments and analyzed preliminary results. All authors analyzed the final results. The manuscript was written from the contributions of all authors.

Conflicts of interest

There are no conflicts to declare.

Acknowledgements

We acknowledge the Research Foundation – Flanders (FWO) (projects AUGE/11/029 and 1275221N) for funding. We thank Mr Laurens Bourda for powder X-ray diffraction measurements.

Notes and references

1 (*a*) E. Ahmed, D. P. Karothu and P. Naumov, *Angew. Chem., Int. Ed.*, 2018, **57**, 8837; (*b*) P. Naumov, D. P. Karothu, E. Ahmed, L. Catalano, P. Commins, J. M. Halabi, M. B. Al-Handawi and L. Li, *J. Am. Chem. Soc.*, 2020, **142**, 13256; (*c*) S. Saha, M. K. Mishra, C. M. Reddy and G. R. Desiraju, *Acc. Chem. Res.*, 2018, **51**, 2957.

2 (*a*) A. J. Thompson, A. I. C. Orue, A. J. Nair, J. R. Price, J. McMurtrie and J. K. Clegg, *Chem. Soc. Rev.*, 2021, **50**, 11725; (*b*) A. Hasija and D. Chopra, *CrystEngComm*, 2021, **23**, 5711; (*c*) A. Hasija, S. Bhandary and D. Chopra, *Cryst. Growth Des.*, 2022, **22**, 2058.

3 (*a*) A. Worthy, A. Grosjean, M. C. Pfrunder, Y. Xu, C. Yan, G. Edwards, J. K. Clegg and J. C. McMurtrie, *Nat. Chem.*, 2018, **10**, 65; (*b*) S. Bhandary, A. J. Thompson, J. C. McMurtrie, J. K. Clegg, P. Ghosh, S. Mangalampalli, S. Takamizawa and D. Chopra, *Chem. Commun.*, 2020, **56**, 12841; (*c*) K. L. Wang, M. K. Mishra and C. C. Sun, *Chem. Mater.*, 2019, **31**, 1794; (*d*) S. Takamizawa and Y. Takasaki, *Chem. Sci.*, 2016, **7**, 1527.

4 (*a*) M. Annadhasan, A. R. Agrawal, S. Bhunia, V. V. Pradeep, S. S. Zade, C. M. Reddy and R. Chandrasekar, *Angew. Chem., Int. Ed.*, 2020, **59**, 13852; (*b*) M. Annadhasan, S. Basak, N. Chandrasekhar and R. Chandrasekar, *Adv. Opt. Mater.*, 2020, **8**, 2000959; (*c*) B. Tang, B. Liu, H. Liu and H. Zhang, *Adv. Funct. Mater.*, 2020, **30**, 2004116; (*d*) T. Seki, N. Hoshino, Y. Suzuki and S. Hayashi, *CrystEngComm*, 2021, **23**, 5686; (*e*) J. Peng, J. Bai, X. Cao, J. He, W. Xu and J. Jia, *Chem.–Eur. J.*, 2021, **27**, 16036; (*f*) K. Naim, M. Singh, S. Sharma, R. V. Nair, P. Venugopalan, S. C. Sahoo and P. P. Neelakandan, *Chem.–Eur. J.*, 2020, **26**, 11979; (*g*) C. Zhang, H. Dong, C. Zhang, Y. Fan, J. Yao and Y. S. Zhao, *Sci. Adv.*, 2021, **7**, eabh3530; (*h*) F. F. Xu, Y. J. Li, Y. Lv, H. Dong, X. Lin, K. Wang, J. Yao and Y. S. Zhao, *CCS Chem.*, 2020, **2**, 369.

5 (*a*) S. Hayashi and T. Koizumi, *Angew. Chem., Int. Ed.*, 2016, **55**, 2701; (*b*) S. Hayashi, F. Ishiwari, T. Fukushima, S. Mikage, Y. Imamura, M. Tashiro and M. Katouda, *Angew. Chem., Int. Ed.*, 2020, **59**, 16195; (*c*) B. Bhattacharya, D. Roy, S. Dey, A. Puthuvakkal, S. Bhunia, S. Mondal, R. Chowdhury, M. Bhattacharya, M. Mandal, K. Manoj, P. K. Mandal and C. M. Reddy, *Angew. Chem., Int. Ed.*, 2020, **59**, 19878; (*d*) T. Mutai, T. Sasaki, S. Sakamoto, I. Yoshikawa, H. Houjou and S. Takamizawa, *Nat. Commun.*, 2020, **11**, 1824; (*e*) Q. Di, J. Li, Z. Zhang, X. Yu, B. Tang, H. Zhang and H. Zhang, *Chem. Sci.*, 2021, **12**, 15423.

6 (*a*) S. Ito, *Chem. Lett.*, 2021, **50**, 649; (*b*) L. Huang, C. Qian and Z. Ma, *Chem.–Eur. J.*, 2020, **26**, 11914; (*c*) Y. Sagara, S. Yamane, M. Mitani, C. Weder and T. Kato, *Adv. Mater.*, 2016, **28**, 1073; (*d*) C. Wang and Z. Li, *Principles and Applications of Aggregation-Induced Emission*, ed. Y. Tang and B. Z. Tang, Springer Nature Switzerland, Cham, 2019, pp. 141–162.

7 (*a*) M. Godumala, A. V. Kumar and R. Chandrasekar, *J. Mater. Chem. C*, 2021, **9**, 14115; (*b*) H. Liu, Z. Bian, Q. Cheng, L. Lan, Y. Wang and H. Zhang, *Chem. Sci.*, 2019, **10**, 227.

8 (*a*) K. Huang, L. Song, K. Liu, A. Lv, M. Singh, K. Shen, J. Shen, J. Wang, H. Wang, H. Shi, H. Ma, M. Gu, G. Sun, W. Yao, Z. An and W. Huang, *npj Flexible Electron.*, 2021, **5**, 21; (*b*) A. V. Kumar, R. Mehdi, J. Ravi, M. Godumala, M. Annadhasan and R. Chandrasekar, *CrystEngComm*, 2021, **23**, 5774.

9 (*a*) S. Ghosh and C. M. Reddy, *Angew. Chem., Int. Ed.*, 2012, **51**, 10319; (*b*) S. Ghosh, M. K. Mishra, S. B. Kadambi, U. Ramamurty and G. R. Desiraju, *Angew. Chem., Int. Ed.*, 2015, **54**, 2674; (*c*) S. Saha and G. R. Desiraju, *J. Am. Chem. Soc.*, 2017, **139**, 1975.

10 (*a*) S. Hayashi, S. Y. Yamamoto, D. Takeuchi, Y. Ie and K. Takagi, *Angew. Chem., Int. Ed.*, 2018, **57**, 17002; (*b*) S. Hayashi, A. Asano, N. Kamiya, Y. Yokomori, T. Maeda and T. Koizumi, *Sci. Rep.*, 2017, **7**, 9453.

11 (*a*) A. J. Thompson, A. Worthy, A. Grosjean, J. R. Price, J. C. McMurtrie and J. K. Clegg, *CrystEngComm*, 2021, **23**, 5731; (*b*) A. J. Thompson, J. R. Price, J. McMurtrie and J. K. Clegg, *Nat. Commun.*, 2021, **12**, 5983.

12 X. Fang and D. Yan, *Sci. China: Chem.*, 2018, **61**, 397.

13 (*a*) Z. He, W. Zhao, J. W. Y. Lam, Q. Peng, H. Ma, G. Liang, Z. Shuai and B. Z. Tang, *Nat. Commun.*, 2017, **8**, 416; (*b*) B. J. Xu, H. Z. Wu, J. R. Chen, Z. Yang, Z. Y. Yang, Y. C. Wu, Y. Zhang, C. J. Jin, P. Y. Lu, Z. G. Chi, S. W. Liu, J. R. Xu and M. Aldred, *Chem. Sci.*, 2017, **8**, 1909; (*c*) L. Xu, G. Li, T. Xu, W. Zhang, S. Zhang, S. Yin, Z. An and G. He, *Chem. Commun.*, 2018, **54**, 9226.

14 J. M. Gere and B. J. Goodno, *Mechanics of Materials*, Cengage Learning, Stanford, CT, 2013.

15 We could not perform bending induced photophysical study for DBS–Br crystal due to lack of suitable crystal size for the PL measurement.

16 P. R. Spackman, M. J. Turner, J. J. McKinnon, S. K. Wolff, D. J. Grimwood, D. Jayatilaka and M. A. Spackman, *J. Appl. Crystallogr.*, 2021, **54**, 1006. **https://crystalexplorer.net/**.

17 (*a*) M. J. Turner, S. P. Thomas, M. W. Shi, D. Jayatilaka and M. A. Spackman, *Chem. Commun.*, 2015, **51**, 3735; (*b*) D. Dey, S. Bhandary, S. P. Thomas, M. A. Spackman and D. Chopra, *Phys. Chem. Chem. Phys.*, 2016, **18**, 31811.

18 (*a*) A. Bauzá, T. J. Mooibroek and A. Frontera, *ChemPhysChem*, 2015, **16**, 2496; (*b*) P. Scilabra, G. Terraneo and G. Resnati, *Acc. Chem. Res.*, 2019, **52**, 1313.

19 (*a*) A. Forni, E. Lucenti, C. Botta and E. Cariati, *J. Mater. Chem. C*, 2018, **6**, 4603; (*b*) J. Yang, X. Zhen, B. Wang, X. Gao, Z. Ren, J. Wang, Y. Xie, J. Li, Q. Peng, K. Pu and Z. Li, *Nat. Commun.*, 2018, **9**, 840.